OPEN ACCESS

Gaseous dark matter detectors

New Journal of Physics
The open-access journal for physics

Gaseous dark matter detectors

G Sciolla[1] **and C J Martoff**[2]

[1] Massachusetts Institute of Technology, 77 Massachusetts Avenue, Cambridge, MA 02139, USA
[2] Barton Hall, Temple University, 1900 N 13th Street, Philadelphia, PA 19122-6082, USA
E-mail: sciolla@mit.edu and martoff@temple.edu

New Journal of Physics **11** (2009) 105018 (19pp)
Received 22 May 2009
Published 16 October 2009
Online at http://www.njp.org/
doi:10.1088/1367-2630/11/10/105018

Abstract. Dark matter (DM) detectors with directional sensitivity have the potential of yielding an unambiguous positive observation of WIMPs as well as discriminating between galactic DM halo models. In this paper, we introduce the motivation for directional detectors, discuss the experimental techniques that make directional detection possible, and review the status of the experimental effort in this field.

Contents

1. Introduction

Astronomical and cosmological observations have recently shown that dark matter (DM) is responsible for 23% of the energy budget of the universe and 83% of its mass [1]. The most promising candidate for DM is the so-called weakly interacting massive particle (WIMP). The existence of WIMPs is independently suggested by considerations of Big Bang cosmology and theoretical supersymmetric particle phenomenology [2]–[4].

Over the years, many direct detection experiments have been performed to search for nuclear recoils due to elastic scattering of WIMPs off the nuclei in the active volume of the detector. The main challenge for these experiments is to suppress the backgrounds that mimic WIMP-induced nuclear recoils. Today's leading experiments have achieved excellent rejection of electromagnetic backgrounds, i.e. photons, electrons and alpha particles, that have a distinct signature in the detector. However, there are sources of background for which the detector response is nearly identical to that of a WIMP-induced recoil, such as the coherent scattering of neutrinos from the Sun [5], or the elastic scattering of neutrons produced either by natural radioactivity or by high-energy cosmic rays.

While neutron and neutrino interactions do not limit today's experiments, they are expected to become dangerous sources of background when the scale of DM experiments grows to fiducial masses of several tons. In traditional counting experiments, the presence of such backgrounds could undermine the unambiguous identification of a DM signal because neutrinos

are impossible to suppress by shielding and underground neutron backgrounds are notoriously difficult to predict [6].

An unambiguous positive identification of a DM signal even in the presence of unknown amounts of irreducible backgrounds could still be achieved if one could correlate the observation of a nuclear recoil in the detector with some unique astrophysical signature that no background could mimic. This is the idea that motivates directional detection of DM.

1.1. The DM wind

The observed rotation curve of our Galaxy suggests that at the galactic radius of the sun the galactic potential has a significant contribution from DM. The DM distribution in our Galaxy, however, is poorly constrained. A commonly used DM distribution, the standard dark halo model [7], assumes a non-rotating, isothermal sphere extending out to 50 kpc from the galactic center. The DM velocity is described by an Maxwell–Boltzmann distribution with dispersion $\sigma_v = 155\,\mathrm{km\,s^{-1}}$. Concentric with the DM halo is the galactic disc of luminous ordinary matter, rotating with respect to the halo, with an average orbital velocity of about $220\,\mathrm{km\,s^{-1}}$ at the radius of the solar system. Therefore in this model, an observer on Earth would see a wind of DM particles with average velocity of $220\,\mathrm{km\,s^{-1}}$.

The DM wind creates two observable effects. The first was pointed out in 1986 by Drukier *et al* [8], who predicted that the Earth's motion relative to the galactic halo leads to an annual modulation of the rates of interactions observed above a certain threshold in direct detection experiments. In its annual rotation around the Sun, the Earth's orbital velocity has a component that is anti-parallel to the DM wind during the summer, and parallel to it during the winter. As a result, the apparent velocity of the DM wind will increase (decrease) by about 10% in summer (winter), leading to a corresponding increase (decrease) of the observed rates in DM detectors. Unfortunately, this effect is difficult to detect because the seasonal modulation is expected to be small (a few per cent) and very hard to disentangle from other systematic effects, such as the seasonal dependence of background rates. These experimental difficulties cast a shadow on the recent claimed observation of the yearly asymmetry by the DAMA/LIBRA collaboration [9].

A larger modulation of the WIMP signal was pointed out by Spergel [10] in 1988. The Earth spins around its axis with a period of 24 sidereal hours. Because its rotation axis is oriented at 48° with respect to the direction of the DM wind, an observer on Earth sees the average direction of the WIMPs change by 96° every 12 sidereal hours (figure 1). This modulation in arrival direction should be resolvable by a DM directional detector, e.g. a detector able to determine the direction of the DM particles. Most importantly, no known background is correlated with the direction of the DM wind. Therefore, a directional detector could hold the key to the unambiguous observation of DM.

In addition to background rejection, the determination of the direction of the arrival of DM particles can discriminate [11]–[15] between various DM halo distributions including the standard dark halo model, models with streams of WIMPs, the Sikivie late-infall halo model [16]–[18], and other anisotropic models. The discrimination power is further enhanced if a determination of the sense as well as the direction of WIMPs is possible [19]. This capability makes directional detectors unique observatories for underground WIMP astronomy.

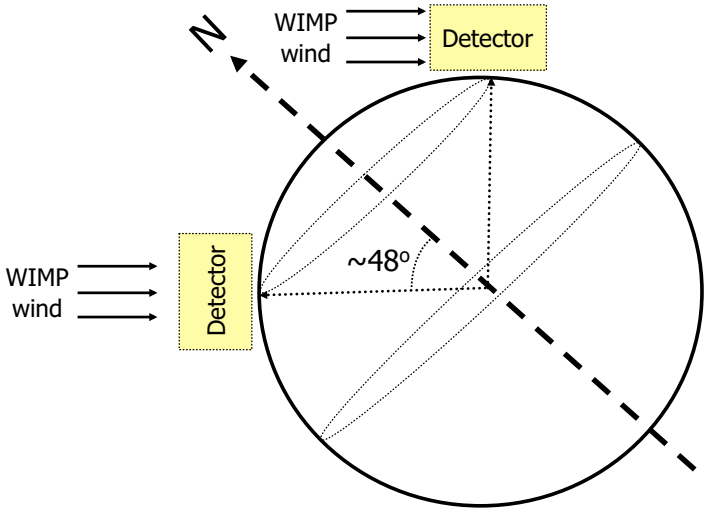

Figure 1. As the Earth spins about its rotation axis, the average direction of the WIMP wind with respect to a DM detector changes by nearly 90° every 12 sidereal hours.

1.2. Directional DM detection

When DM particles interact with regular matter, they scatter elastically off the atoms and generate nuclear recoils with typical energies E_R of a few tens of keV, as explained in more detail in section 2. The direction of the recoiling nucleus encodes the direction of the incoming DM particle. To observe the daily modulation in the direction of the DM wind, an angular resolution of 20–30° in the reconstruction of the recoil nucleus is sufficient, because the intrinsic spread in arrival directions of WIMPs is $\approx 45°$. Assuming that sub-millimeter tracking resolution can be achieved, the length of a recoil track has to be of at least 1–2 mm, which can be obtained by using a very dilute gas as a target material.

An ideal directional detector should provide a three dimensional (3D) vector reconstruction of the recoil track with a spatial resolution of a few hundred microns in each coordinate, and combine a very low-energy threshold with an excellent background rejection capability. Such a detector would be able to reject isotropy of the recoil direction, and hence identify the signature of a WIMP wind, with just a handful of events [13].

More recently, Green and Morgan [19] studied how the number of events necessary to detect the WIMP wind depends on the detector performance in terms of energy threshold, background rates, 2D versus 3D reconstruction of the nuclear recoil, and ability to determine the sense of the direction by discriminating between the 'head' and 'tail' of the recoil track. 'Head–tail' discrimination is obtained by measuring the energy loss ($\mathrm{d}E/\mathrm{d}x$) along the recoil track. The WIMP-induced low-energy recoils are well below the Bragg peak, and therefore $\mathrm{d}E/\mathrm{d}x$ decreases with decreasing energy. The default configuration used for this study assumes a CS_2 gaseous TPC running at 0.05 bar using 200 μm pixel readout providing 3D reconstruction of the nuclear recoil and perfect 'head–tail' discrimination. The energy threshold is assumed to be 20 keV, with perfect background rejection. In such a configuration, seven events would be sufficient to establish observation of the WIMP wind at 90% C.L. In the presence of background with $S/N = 1$, the number of events necessary to reject isotropy would increase by a factor of 2.

If only 2D reconstruction is available, the required number of events doubles compared to the default configuration. 'Head–tail' discrimination turns out to be the most important capability: if the sense cannot be measured, the number of events necessary to observe the effects of the WIMP wind increases by one order of magnitude.

2. Nuclear recoils in gaseous detectors

To optimize the design of gaseous detectors for directional detection of DM one must be able to calculate the recoil atom energy spectrum expected for a range of WIMP parameters and halo models. The detector response in the relevant energy range must also be predictable. The response will be governed first and foremost by the track length and characteristics (multiple scattering) as a function of recoil atom type and energy. Since gas detectors require ionization for detection, design also requires knowledge of the ionization yield in gas and its distribution along the track as a function of recoil atom type and energy, and possibly electric field.

The large momentum transfer necessary to produce a detectable recoil in gas implies that the scattering atom can be treated as a free particle, making calculations of the recoil spectrum essentially independent of whether the target is a solid, liquid or gas.

An estimate of the maximum DM recoil energy for simple halo models is given by the kinematically allowed energy transfer from an infinitely heavy halo WIMP with velocity equal to the galactic escape speed. This speed is locally about 500–600 km s^{-1} [20]; WIMPs with higher velocities than this would not be gravitationally bound in the halo and would presumably be rare. The corresponding maximum energy transfer amounts to <10 keV nucleon^{-1}. The integrated rate will be concentrated at lower energies than this, at least in halo models such as the isothermal sphere. For that model, the recoil energy (E_{R}) distribution [7] is proportional to $\exp(-E_{\mathrm{R}}/E_{\mathrm{I}})$, with E_{I} a constant that depends on the target and WIMP masses and the halo model. For a 100 GeV WIMP and the isothermal halo model parameters of Smith and Lewin [7], E_{I}/A varies from 1.05 to 0.2 keV nucleon^{-1} for target mass numbers from 1 to 131. These are very low-energy particles, well below the Bragg peak at ∼200–800 keV A^{-1}. In this regime $\mathrm{d}E/\mathrm{d}x$ *decreases* with decreasing energy, and the efficiency of ionization is significantly reduced.

2.1. Lindhard model for low-energy stopping

The stopping process for such low-energy particles in homoatomic[3] substances was treated by Lindhard, Scharff and Schiott (LSS) [21, 22]. This treatment has stood the test of time and experiment, making it worthwhile to summarize the results here.

As is now well known, the primary energy loss mechanisms for low-energy particles in matter can be divided into 'nuclear stopping', due to atom–atom scattering, and 'electronic stopping', due to atom–electron scattering. These mechanisms refer only to the initial interaction causing the incident particle to lose energy. Nuclear stopping eventually contributes to electronic excitations and ionization, and electronic stopping eventually contributes to thermal excitations [22].

In [21], the stopping is described using a Thomas–Fermi atom model to obtain numerical results for universal stopping-power curves in terms of two variables, the scaled energy

[3] A homoatomic molecular entity is a molecular entity consisting of one or more atoms of the same element.

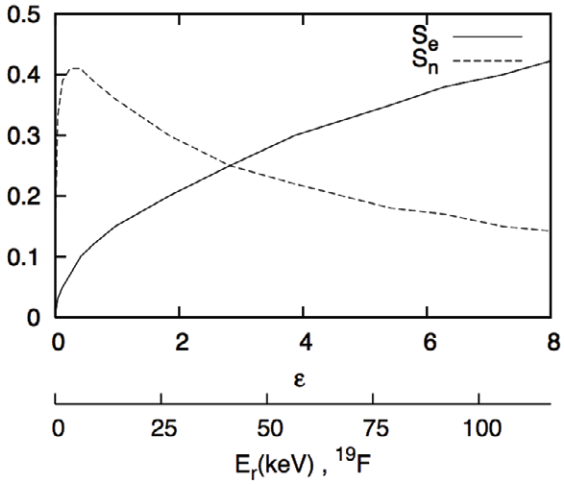

Figure 2. LSS electronic (S_e) and nuclear (S_n) stopping as a function of scaled energy ϵ. The vertical axis is in LSS units of $d\epsilon/d\rho$ where ρ is the scaled range in an assumed solid absorber. The energy axis for homoatomic recoils of ^{19}F is also shown.

$\epsilon = E_R/E_{TF}$, and the scaled range $\rho = R/R_{TF}$, where E_R and R are, respectively, the energy and the stopping distance of the recoil, and E_{TF} and R_{TF} are scale factors[4].

Figure 2 shows that nuclear stopping dominates in the energy range where most of the rate for DM detection lies. This can be seen as follows. The scaled variables ϵ and ρ depend algebraically on the atomic numbers and mass numbers of the incident and target particles. The scale factor E_{TF} corresponds to 0.45 keV nucleon^{-1} for homoatomic recoils in carbon, 1.7 keV nucleon^{-1} for Ar in Ar and 6.9 keV nucleon^{-1} for Xe in Xe. Nuclear stopping $\frac{d\epsilon_n}{d\rho}$ was found to be larger than the electronic stopping $\frac{d\epsilon_e}{d\rho}$ for $\epsilon < 1.6$, which covers the energy range $0 < E_R < E_I$ where most of the DM recoil rate can be expected.

Because of the dominance of nuclear stopping, detectors can be expected to respond differently to DM recoils than to radiations such as x-rays or even α particles, for which electronic stopping dominates. Nuclear stopping yields less ionization and electronic excitation per unit energy loss than does electronic stopping, implying that the W factor, defined as the energy loss required to create one ionization electron, will be larger for nuclear recoils. Lindhard *et al* [22] present calculations of the ultimate energy loss partitioning between electronic and atomic motion. Experimenters use empirical 'quenching factors' to describe the variation of energy per unit of ionization (the 'W' parameter) compared with that from x-rays.

The different microscopic distribution of ionization in tracks dominated by nuclear stopping can also lead to unexpected changes in the interactions of ionized and electronically excited target atoms (e.g. dimer formation, recombination). Such interactions are important for particle identification signatures such as the quantity and pulse shape of scintillation light output, the variation of scintillation pulse shape with applied electric field, and the field variation of ionization charge collection efficiency. Such effects are observed in gases [23, 24], and even more strongly in liquid and solid targets [25].

[4] The scale factors are (in cgs-Gaussian units): $E_{TF} = \frac{e^2}{a} Z_i Z_T \frac{M_i+M_T}{M_T}$, $R_{TF} = \frac{1}{4\pi a^2 N} \frac{(M_i+M_T)^2}{M_i M_T}$. Here, N = number density of target atoms, subscripts i and T refer to the incident particle and the target substance, and $a = a_0 \frac{0.8853}{\sqrt{Z_i^{2/3}+Z_T^{2/3}}}$, with a_0 the Bohr radius.

Electronic stopping [21] was found to vary as $\frac{d\epsilon_e}{d\rho} = k\sqrt{\epsilon}$ with the parameter k varying only from 0.13 to 0.17 for homonuclear recoils in $A = 1$ to 131.[5] Let us define the total stopping as $\frac{d\epsilon}{d\rho} = \frac{d\epsilon_n}{d\rho} + \frac{d\epsilon_e}{d\rho}$ and the total scaled range as $\rho_o = \int_0^{\epsilon} \frac{d\epsilon}{(\frac{d\epsilon}{d\rho})}$. The relatively small contribution of electronic stopping and the small variation in k for homoatomic recoils, makes the total scaled range for this case depend on the target and projectile almost entirely through E_{TF}.

Predictions for the actual range of homoatomic recoils can be obtained from the nearly universal scaled range curve as follows. Numerically, integrating the stopping curves of Lindhard *et al* [21] with k set to 0.15 gives a scaled range curve that fits the surprisingly simple expression

$$\rho_o \doteq 2.04\epsilon + 0.04 \tag{1}$$

with accuracy better than 10% for $0.12 < \epsilon < 10$. According to the formula given earlier, the scale factor R_{TF} lies between 1 and 4×10^{17} atoms cm^{-2} for homoatomic recoils in targets with $12 \leqslant A \leqslant 131$. Thus the model predicts ranges of several times 10^{17} atoms cm^{-2} at $E_R = E_I$. This is of the order of a few millimeters for a monoatomic gas at 0.05 bar. As a consequence, tracking devices for the DM detection must provide accurate reconstruction of tracks with typical lengths between 1 and a few millimeters while operating at pressures of a small fraction of an atmosphere. The range calculated by integrating the LSS stopping powers is shown in figure 3.

When comparing LSS predictions with experimental results, two correction factors must be considered. First, the widely used program SRIM [26] produces range-energy tables that contain the 'projected range', while LSS calculate the path length along the track. On the other hand, many older experiments report 'extrapolated ranges', which are closer in magnitude to the path length than to the 'projected range'. To compare the SRIM tables with LSS, the projected range should be multiplied by a factor [21] $(1 + \frac{M_T}{3M_P})$, where M_T and M_P are the target and projectile masses. This correction has generally been applied in the next section, where experimental data are discussed.

In addition, it must be noted that the LSS calculations described above were obtained for solids. Therefore, one should consider a gas–solid correction in ranges and stopping powers, as discussed by Bohr *et al* [27]. In condensed phases, the higher collision frequency results in a higher probability for stripping of excited electrons before they can relax, which leads to a higher energy loss rate than for gases. This correction is rather uncertain and has generally not been applied in the following section of this paper.

Finally, numerical calculations to extend the LSS model to the case of targets of mixed atomic number are given in [28].

2.2. *Experimental data on low-energy stopping in gases*

The literature of energy loss and stopping of fast particles in matter is vast and still growing [29, 30]. However, there is not a lot of experimental data available for particle ranges and ionization yields in gas at the very low energies typical of DM recoils, where $E/A \sim 1$ keV nucleon^{-1}. Comprehensive collections of citations for all energies are available [26, 31], upon which the widely used theory-guided-fitting computer programs SRIM and MSTAR [31] are based.

[5] The parameter $k \doteq \frac{0.0793 Z_1^{1/6}}{(Z_1^{2/3}+Z_2^{2/3})^{3/4}} \left[\frac{Z_1 Z_2 (A_1+A_2)^3}{A_1^3 A_2}\right]^{1/2}$ becomes substantially larger only for light recoils in heavy targets.

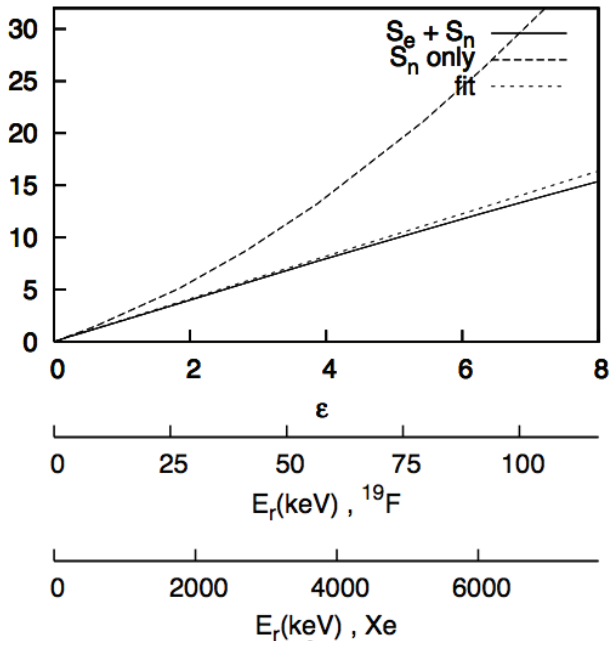

Figure 3. LSS range as a function of scaled energy ϵ. The vertical axis is in LSS units of scaled range ρ in an assumed solid absorber. The curves shown are from integration of the nuclear plus electronic $(S_e + S_n)$ stopping with $k = 0.15$, the nuclear stopping only (S_n), and the fit referred to in the text. The energy axes for homoatomic ^{19}F and ^{131}Xe recoils are also shown. Multiply the vertical axis values by 3.6 to get approximate range in $\mu g\,cm^{-2}$ for F in CF_4 estimated by averaging the Z and A values for the constituent atoms. Multiply the vertical axis values by 90 to get range in $\mu g\,cm^{-2}$ for Xe.

Several older papers [32]–[34] still appear representative of the available direct measurements at very low energy. More recent studies [35] provide indirect information based on large detector simulations.

Both [32] and [33] used accelerated beams of He, N, Ne, Ar and ^{24}Na, ^{66}Ga and ^{198}Au in differentially pumped gas target chambers filled with pure-element gases. In [32], the particles were detected with an ionization chamber, while in [33] radioactive beams were used. The stopped particles were collected on segmented walls of the target chamber and later counted. Typical results were ranges of $2(3.2) \times 10^{17}$ atoms cm^{-2} for 26(40) keV Ar^+ in argon. The fit to LSS theory given above predicts ranges that are shorter than the experimental results by 10–40%, which is consistent with experimental comparisons given by LSS. Accuracy of agreement with the prediction from the SRIM code is about the same. As in all other cases discussed below, the direction of the deviation from LSS is as expected from the gas–solid effect mentioned in the previous section.

In [35], nuclear recoils from ^{252}Cf neutrons were recorded by a negative ion time projection chamber (NITPC) filled with 40 Torr CS_2. The device was simulated fitting the observed pulse height and event size distributions. The best fit range curves given for C and S recoils in the gas are 10–20% higher at 25–100 keV than LSS predictions computed by the present authors by assuming simple additivity of stopping powers for the constituent atoms of the polyatomic gas target.

2.3. Ionization yields

Tracking readouts in gas TPC detectors are sensitive only to ionization of the gas. As noted above, both nuclear stopping and electronic stopping eventually contribute to both electronic excitations (including ionization) and to kinetic energy of target atoms, as primary and subsequent generations of collision products interact further with the medium. Some guidance useful for design purposes is available from [22], where the energy cascade was treated numerically using integral equations. In terms of the scaled energy ϵ and the electronic stopping coefficient k introduced above, the (scaled) energy η ultimately transferred to electrons was found to be well approximated [36] by $\eta = \frac{\epsilon}{1+\frac{1}{kg(\epsilon)}}$ with $g(\epsilon) = \epsilon + 3\epsilon^{0.15} + 0.7\epsilon^{0.6}$. This function interpolates smoothly from $\eta = 0$ at $\epsilon = 0$ to $\eta = \epsilon$ for $\epsilon \to \infty$, giving $\eta = 0.4$ at $\epsilon = 1$. In other words, this theory predicts only about 40% as much ionization per unit of energy deposited by DM recoils as by low LET radiation such as electrons ejected by x-rays.

Several direct measurements of total ionization by very low-energy particles are available in the literature. Many of these results are for recoil nuclei from alpha decays [34, 37, 38]. These $\sim$100 keV, $A \sim 200$ recoils are of interest as backgrounds in DM experiments, but their scaled energy $\epsilon \cong 0.07$ is below the range of interest for most WIMP recoils. Measured ionization yield parameters W were typically 100–120 eV ion^{-1} pair, in good agreement with the approximate formula for η given above. Data more applicable to DM recoils are given in [39]–[42]. Some representative results from these works include [40] $W = 91$ (65) eV IP^{-1} for 25 (100) keV Ar in Ar, both values about 20% higher than would be predicted by the preceding approximate LSS expression. Higher W for gases than for condensed media is expected [27] as mentioned above. Mc Donald and Sideneus [41] measured total ionization from particles with $1 < Z < 22$ in methane. While in principle the LSS treatment does not apply to heteroatomic gases, using the LSS prescription to predict the W factor for a carbon target (rather than methane) yields a value that is about 15% lower than the experimental results.

The authors of [35] also fit their data to derive W-values for C and S recoils. Their best-fit values are again 10–25% higher than an LSS-based estimate by the present author using additivity.

To summarize, most of the DM recoils expected from an isothermal galactic halo have very low energies, and therefore nuclear stopping plays an important role. The sparse available experimental data on track lengths and ionization yields agrees at the $\sim$20% level with simple approximate formulae based on the Lindhard model. Without applying any gas-phase correction, LSS-based estimates for range tend to be slightly shorter than those experimentally measured in gases. The predicted ionization parameter W also tends to be slightly lower than the experimental data. This situation is adequate for initial design of detectors, but with the present literature base, each individual experiment will require its own dedicated calibration measurements.

3. Considerations for directional detector design

3.1. Detector architecture

From the range-energy discussion in the previous section, we infer that track lengths of typical DM recoils will be only of the order of 0.1 μm in condensed matter, while track lengths of up to a few millimeters are expected in gas at a tenth of the atmospheric pressure. Several

techniques relevant to direction-sensitive detection using condensed matter targets have been reported, including track-etch analysis of ancient mica [43], bolometric detection of surface sputtered atoms [44], and use of nuclear emulsions [45]. The ancient mica etch pit technique was actually used to obtain DM limits. However, recently the focus of directional DM detection has shifted to low-pressure gas targets, and that is the topic of the present review.

The TPC [46, 47] is the natural detector architecture for gaseous direction-sensitive DM detectors, and essentially all experiments use this configuration. The active target volume contains only the active gas, free of background-producing material. Only one wall of the active volume requires a readout system, leading to favorable cost-volume scaling. TPCs with nearly $100\,\mathrm{m}^3$ of active volume have been built for high-energy physics, showing the possibility of large active masses.

3.2. Background rejection capabilities

Gaseous DM detectors have excellent background rejection capability for different kinds of backgrounds. First and foremost, direction sensitivity gives gas detectors the capability of statistically rejecting neutron and neutrino backgrounds. In addition, tracking also leads to extremely effective discrimination against x- and γ-rays backgrounds [48, 49]. The energy loss rates for recoils discussed in the previous section are hundreds of times larger than those of electrons with comparable total energy. The resulting much longer electron tracks are easily identified and rejected in any direction-sensitive detector. Finally, the measured rejection factors for gamma rays versus nuclear recoils varies between 10^4 and 10^6 depending on the experiment [35, 50, 51].

3.3. Choice of pressure

It can be shown that there is an optimum pressure for operation of any given direction sensitive WIMP recoil detector. This optimum pressure depends on the fill gas, the halo parameter set and WIMP mass, and the expected track length threshold for direction measurement.

The total sensitive mass, and hence the total number of expected events, increases proportionally to the product of the pressure P and the active volume V. Equation (1) above shows that the range in atoms cm^{-2} for WIMP recoils is approximately proportional to their energy. Since the corresponding range in centimeter is inversely proportional to the pressure ($R \propto E_\mathrm{r}/P$), the energy threshold imposed by a particular minimum track length $E_{\mathrm{r,min}}$ will scale down linearly with decreasing pressure, $E_{\mathrm{r,min}} \propto R_{\mathrm{min}} P$, where R_{min} is the shortest detectable track length. For the exponentially falling recoil energy spectrum of the isothermal halo [36] the fraction of recoils above a given energy threshold is proportional to $\exp(-E_{\mathrm{min}}/E_0 r)$. Hence the rate of tracks longer than the tracking threshold $\mathrm{R}_{\mathrm{min}}$ will scale as $N \propto PV\exp(-\xi R_{\mathrm{min}} P)$, with ξ a track length factor depending on the target gas, WIMP mass, halo model, etc, and the track length threshold R_{min} depending on the readout technology and the drift distance. This expression has a maximum at $P_{\mathrm{opt}} = 1/[\xi R_{\mathrm{min}}]$, which shows that the highest event rate is obtained by taking advantage of improvement in tracking threshold to run at higher target pressure. Operating at this optimum pressure, the track-able event rate still scales as $P_{\mathrm{opt}} V$, which increases linearly as the tracking threshold decreases. Achieving the shortest possible tracking threshold R_{min} is seen to be the key to sensitive experiments of this type.

3.4. Tracking limit due to diffusion

Diffusion of track charge during its drift to the readout plane sets the ultimate limit on how short a track can be measured in a TPC. Diffusion in gases has a rich phenomenology for which only a simplified discussion is given here. More complete discussion with references to the literature is given by Rolandi and Blum [52].

For low values of electric fields, elementary kinetic theory arguments predict equal transverse and longitudinal diffusion to the drift field E_d, with the rms diffusion spread δ given by

$$\delta = \sqrt{\frac{2kTL}{eE_\mathrm{d}}} = 0.7\,\mathrm{mm}\sqrt{\frac{[L/1\mathrm{m}]}{[E_\mathrm{d}/1\,\mathrm{kV/cm}]}}. \tag{2}$$

Here k is the Boltzmann constant, T the gas temperature, and L the drift distance. No pressure or gas dependence appears in this equation. The diffusion decreases inversely as the square root of the applied drift field. Increasing the drift field would appear to allow diffusion to be reduced as much as desired, allowing large detectors to be built while preserving good tracking resolution.

However, in reality diffusion is not so easily controlled. The low-field approximation given by equation (2) holds only below a certain maximum drift field value $E_\mathrm{d}^\mathrm{max}$, which depends on the pressure and target gas. The drift field must not violate the condition $eE_\mathrm{d}^\mathrm{max}\lambda \ll kT$, where the effective mean free path $\lambda = 1/fn\sigma$ decreases inversely as the pressure. Here σ is the average total cross section for scattering of the drifting species on the fill gas molecules, n is the number density of molecules, and f is an energy-exchange-efficiency factor for the scattering of charge carriers from gas molecules. This condition amounts to requiring that the work done by the drift field on a charge carrier between collisions and not lost to collisions, must be much smaller than the carrier's thermal energy. If this condition is fulfilled it will ensure that the drifting carriers' random (thermal) velocity remains consistent with the bulk gas temperature. A larger scattering cross section σ or a more effective energy exchange due to strong inelastic scattering processes will lead to a shorter effective mean free path and a larger value of $E_\mathrm{d}^\mathrm{max}$. Importantly, $E_\mathrm{d}^\mathrm{max}$ for electrons in a given gas generally scales inversely as the pressure, as would be expected from the presence of the mean free path in the 'low field' condition.

If the drift field exceeds $E_\mathrm{d}^\mathrm{max}$, the energy gained from the drift field becomes non-negligible. The average energy of drifting charge carriers begins to increase appreciably, giving them an effective temperature T_eff, which can be orders of magnitude larger than that of the bulk gas. Under these conditions, the kinetic theory arguments underlying equation (2) remain approximately valid if the gas temperature T is replaced by T_eff. Diffusion stops dropping with increasing drift field and may rapidly *increase* in this regime, with longitudinal diffusion increasing more rapidly than transverse.

Values of $E_\mathrm{d}^\mathrm{max}/P$ for electrons drifting in various gases and gas mixtures vary from $\sim$0.1–1 V cm^{-1} Torr^{-1} at 300 K [53, 54]. With drift fields limited to this range and a gas pressure of $\sim$50 Torr, the rms diffusion for a 1 m drift distance would be several millimeters, severely degrading the tracking resolution.

Effects of diffusion can be significantly reduced by drifting negative ions instead of electrons [55]–[57]. Electronegative vapors have been found which, when mixed into detector gases, reversibly capture primary ionization electrons within $\sim$100 μm of their creation. The resulting negative ions drift to the gain region of the chamber, where collisional processes

free the electrons and initiate normal Townsend avalanches [58]. Ions have $E_{\mathrm{d}}^{\max}$ values corresponding to $E/P = 20\,\mathrm{V\,cm^{-1}\,Torr^{-1}}$ and higher. This is because the ions' masses are comparable to the gas molecules, so the energy-exchange-efficiency factor f, which determines $E_{\mathrm{d}}^{\max}$ is much larger than for electrons. Ion–molecule scattering cross sections also tend to be larger than electron–molecule cross sections. The use of negative ion drift in TPCs would allow sub-millimeter rms diffusion for drift distances of 1 m or larger, although total drift voltage differences in the neighborhood of 100 kV would be required.

The above outline shows that diffusion places serious constraints on the design of detectors with large sensitive mass and millimeter track resolution, particularly when using a conventional electron drift TPC.

3.5. Challenges of directional detection

The current limits on spin-independent interactions of WIMPs in the $60\,\mathrm{GeV\,c^{-2}}$ mass range have been set using 300–400 kg-day exposures, for example by the XENON10 [59] and CDMS [60] experiments. Next generation non-directional experiments are being planned to achieve zero background with hundreds or thousands of times larger exposures [61].

To be competitive, directional detectors should be able to use comparable exposures. However, integrating large exposures is particularly difficult for low-pressure gaseous detectors. A fiducial mass of a few tons will be necessary to observe DM-induced nuclear recoils for much of the theoretically favored range of parameter space [4]. This mass of low-pressure gas would occupy thousands of cubic meters. It is, therefore, key to the success of the directional DM program to develop detectors with a low cost per unit volume. Since for standard gaseous detectors the largest expense is represented by the cost of the readout electronics, it follows that a low-cost readout is essential to make DM directional detectors financially viable.

4. DM TPC experiments

4.1. Early history of direction-sensitive WIMP detectors

As early as 1990, Gerbier *et al* [62] discussed using a hydrogen-filled TPC at 0.02 bar, drifting electrons in a 0.1 T magnetic field to detect proton recoils from DM collisions. This proposal was made in the context of the 'cosmion', a then-current WIMP candidate with very large ($10^{-36}\,\mathrm{cm^2}$) cross section for scattering on protons. These authors explicitly considered the directional signature, but they did not publish any experimental findings.

A few years later, the UCSD group led by Masek [63] published results of early trials of the first detector system specifically designed for a direction-sensitive DM search. This pioneering work used optical readout of light produced in a parallel plate avalanche counter (PPAC) located at the readout plane of a low-pressure TPC. The minimum discernible track length was about 5 mm. Electron diffusion at low pressures and its importance for the performance of gas detectors was also studied [64]. This early work presaged some of the most recent developments in the field, described in section 4.4.

4.2. DRIFT

The DRIFT-I collaboration [48] mounted the first underground experiment designed for direction sensitive WIMP recoil detection [65]. Redesigned detectors were built and further

characterization measurements were performed by the DRIFT-II [66] collaboration. Both DRIFT detectors were cubical 1 m^3 negative-ion-drifting TPCs with two back-to-back 0.5 m drift spaces. To minimize material possibly contributing radioactive backgrounds, the central drift cathode was designed as a plane of 20 μm wires on 2 mm pitch. The endcap MWPCs used 20 μm anode wires on 2 mm-pitch, read out with transient digitizers. In DRIFT-II, the induced signals on grid wires between the MWPC anode and the drift space were also digitized. DRIFT-I had an amplifier- and digitizer-per-wire readout, while DRIFT-II signals were cyclically grouped onto a small number of amplifiers and digitizers. Both detectors used the negative ion drift gas CS_2 at nominally 40 Torr, about one-twentieth of the atmospheric pressure. The 1 m^3 volume gave approximately 170 g of target mass per TPC. The CS_2 gas fill allowed diffusion suppression by running with very high drift fields despite the low pressure. DRIFT-II used drift fields up to 624 V cm^{-1}(16 V cm^{-1} $Torr^{-1}$).

The detectors were calibrated with alpha particles, ^{55}Fe x-rays and ^{252}Cf neutrons. Alpha particle Bragg peaks and neutron recoil events from sources were quickly seen after turn-on of DRIFT-I underground in 2001. Neutron exposures gave energy spectra in agreement with simulations when the energy per ion pair W was adjusted in accordance with the discussion of ionization yields given above. Simulations of DRIFT-II showed that the detector and software analysis chain had about 94% efficiency for detection of those ^{252}Cf neutron recoils producing between 1000 and 6000 primary ion pairs, and a ^{60}Co gamma-ray rejection ratio better than a few times 10^{-6} [67]. A study of the direction sensitivity of DRIFT-II for neutron recoils [68] showed that a statistical signal distinguishing the beginning and end of sulfur recoil tracks ('head–tail discrimination') was available, although its energy range and statistical power was limited by the 2 mm readout pitch.

At present two 1 m^3 DRIFT-II modules are operating underground. Backgrounds due to radon daughters implanted in the internal surfaces of the detector [67] are under study and methods for their mitigation are being developed. The absence of nonzero spin nuclides in the CS_2 will require a very large increase in target mass or a change of gas fill in order to detect WIMPs with this device.

4.3. DM searches using micropattern gas-gain devices

It was shown above that the event rate and therefore the sensitivity of an optimized tracking detector improves linearly as the track length threshold gets smaller. In recent years, there has been widespread development of gas detectors achieving very high spatial resolution by using micropatterned gain elements in place of wires. For a recent overview of micropattern detector activity, see [69]. These devices typically have 2D arrays of individual gain elements on a pitch of ∼0.1 mm. Rows of elements [70] or individual gain elements can be read out by suitable arrangements of pickup electrodes separate from the gain structures, or by amplifier-per-pixel electronics integrated with the gain structure [71]. Gain-producing structures known as gas electron multiplier (GEM) [72] and MICRO-MEsh GAseous structure (MicroMegas) [73] have found particularly wide application.

The gas CF_4 also figures prominently in recent micropattern DM search proposals. This gas was used for low background work in the MUNU experiment [74] and has the advantage of high E_d^{max}, allowing relatively low diffusion for electron drift at high drift field and reduced pressure [54, 75, 76], although it does not approach negative ions in this regard. Containing the odd-proton nuclide ^{19}F is also an advantage since it confers sensitivity to purely

spin-coupled WIMPs [77], allowing smaller active mass experiments to be competitive. Another attractive feature of CF_4 is that its Townsend avalanches copiously emit visible and near-infrared light [78]–[80], allowing optical readout as in the DMTPC detector discussed in section 4.4. The ultraviolet part of the spectrum may also be seen by making use of a wavelength shifter. Finally, CF_4 is non-flammable and non-toxic, and, therefore, safe to operate underground.

The NEWAGE project is a current DM search program led by a Kyoto University group. This group has recently published the first limit on DM interactions derived from the absence of a directional modulation during a 0.15 kg-day exposure [50]. NEWAGE uses CF_4-filled TPCs with a microwell gain structure [81]–[83]. The detector had an active volume of $23 \times 28 \times 30\,\mathrm{cm}^3$ and contained CF_4 at 150 Torr. Operation at higher-than-optimal gas pressure was chosen to enhance the HV stability of the gain structure. The chamber was read out by a single detector board referred to as a 'μ-PIC', preceded by a GEM for extra gas gain.

The μ-PIC has a micro-well gain structure produced using multi-layer printed circuit board technology. It is read out on two orthogonal, 400 μm-pitch arrays of strips. One array is connected to the central anode dots of the micro-well gain structure, and the other array to the surrounding cathodes. The strip amplifiers and position decoding electronics are on-board with the gain structures themselves, using an eight layer PCB structure.

The detector was calibrated with a ^{252}Cf neutron source. Nuclear recoils were detected and compared to a simulation, giving a detection efficiency rising from zero at 50 keV to 90% near 250 keV. For comparison, the maximum energy of a ^{19}F recoil from an infinitely heavy WIMP with the galactic escape speed is about 180 keV. The measured rejection factor for ^{137}Cs gamma rays was about 10^{-4}. The angular resolution was reported as 25° HWHM. Measurement of the forward/backward sense of the tracks ('head–tail' discrimination) was not reported.

Another gaseous DM search collaboration known as MIMAC [84] is led by a group at IPN Grenoble, and has reported work toward an electronically read-out direction sensitive detector. They proposed the use of ^{3}He mixtures with isobutane near 1 bar, and also CF_4 gas fills to check the dependence on the atomic number A of any candidate DM signal. The advantages claimed for ^{3}He as a DM search target include nonzero nuclear spin, low mass and hence sensitivity to low WIMP masses, and a very low Compton cross section, which suppresses backgrounds from gamma rays. The characteristic (n, p) capture interaction with slow neutrons gives a strong signature for the presence of slow neutrons. The ionization efficiency of $\sim$1 keV ^{3}He recoils is also expected to be very high, allowing efficient detection of the small energy releases expected for this target and for light WIMPs. A micropattern TPC with $\sim$350 μm anode pitch was proposed to obtain the desired electron rejection factor at a few keV. The MIMAC collaboration uses an ion source to generate monoenergetic ^{3}He and F ions for measuring the ionization yield in their gas mixtures [85].

4.4. Dark matter time projection chamber (DMTPC)

The DMTPC collaboration has developed a new detector concept [49] that addresses the issue of scalability of directional DM detectors by using optical readout, a potentially very inexpensive readout solution.

The DMTPC detector [86, 87] is a low-pressure TPC filled with CF_4 at a nominal pressure of 50 Torr (figure 4). The detector is read out by an array of CCD cameras and photomultipliers (PMTs) mounted outside the vessel to reduce the amount of radioactive material in the active volume. The CCD cameras image the visible and near infrared photons that are produced by

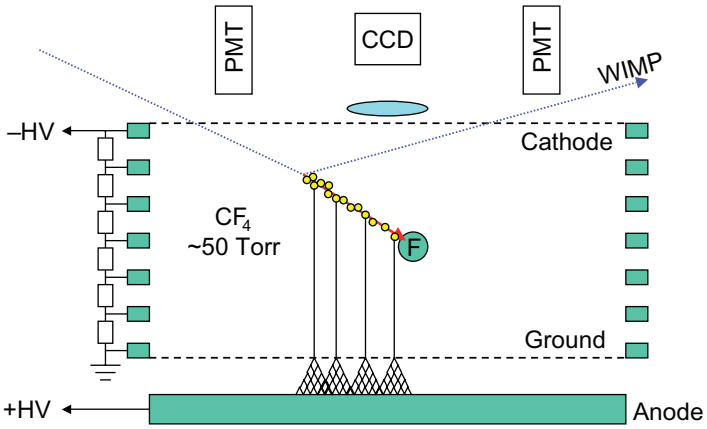

Figure 4. Illustration of the DMTPC detector concept.

the avalanche process in the amplification region, providing a projection of the 3D nuclear recoil on the 2D amplification plane. The 3D track length and direction of the recoiling nucleus is reconstructed by combining the measurement of the projection along the amplification plane (from pattern recognition in the CCD) with the projection along the direction of drift, determined from the waveform of the signal from the PMTs. The sense of the recoil track is determined by measuring $\mathrm{d}E/\mathrm{d}x$ along the length of the track. The correlation between the energy of the recoil, proportional to the number of photons collected in the CCD, and the length of the recoil track provides an excellent rejection of all electromagnetic backgrounds.

Several alternative implementations of the amplification region [51] were developed. In a first design, the amplification was obtained by applying a large potential difference ($\Delta V =$ 0.6–1.1 kV) between a copper plate and a conductive woven mesh kept at a uniform distance of 0.5 mm. The copper or stainless steel mesh was made of 28 μm wire with a pitch of 256 μm. In a second design the copper plate was replaced with two additional woven meshes. This design has the advantage of creating a transparent amplification region, which allows a substantial cost reduction since a single CCD camera can image tracks originating in two drift regions located on either side of a single amplification region.

The current DMTPC prototype [88] consists of two optically independent regions contained in one stainless steel vessel. Each region is a cylinder with 30 cm diameter and 20 cm height contained inside a field cage. Gas gain is obtained using the mesh-plate design described above. The detector is read out by two CCD cameras, each imaging one drift region. Two $f/1.255$ mm Nikon photographic lenses focus light onto two commercial Apogee U6 CCD cameras equipped with Kodak 1001E CCD chips. Because the total area imaged is $16 \times 16\,\mathrm{cm}^2$, the detector has an active volume of about 10 liters. For WIMP-induced nuclear recoils of 50 keV, the energy and angular resolutions obtained with the CCD readout were estimated to be $\approx 15\%$ and 25°, respectively. This apparatus is currently being operated above ground with the goal of characterizing the detector response and understanding its backgrounds. A second 10-liter module is being constructed for underground operations at the waste isolation pilot plant (WIPP) in New Mexico.

A 5.5 MeV alpha source from ^{241}Am is used to study the gain of the detector as a function of the voltage and gas pressure, as well as to measure the resolution as a function of the drift distance of the primary electrons to quantify the effect of the transverse diffusion. These

studies [54, 75] show that the transverse diffusion allows for a sub-millimeter spatial resolution in the reconstruction of the recoil track for drift distances up to 20–25 cm. The gamma ray rejection factor, measured using a ^{137}Cs source, is better than 2 parts per million [75].

The performance of the DMTPC detector in determining the sense and direction of nuclear recoils has been evaluated by studying the recoil of fluorine nuclei in interaction with low-energy neutrons. The initial measurements were obtained running the chamber at 280 Torr and using 14 MeV neutrons from a deuteron–triton generator and a ^{252}Cf source. The 'head–tail' effect was clearly observed [75, 89] for nuclear recoils with energy between 200 and 800 keV. Better sensitivity to lower energy thresholds was achieved by using higher gains and lowering the CF_4 pressure to 75 Torr. These measurements demonstrated [51] 'head–tail' discrimination for recoils above 100 keV, and reported a good agreement with the predictions of the SRIM [26] simulation. 'Head–tail' discrimination is expected to extend to recoils above 50 keV when the detector is operated at a pressure of 50 Torr. To evaluate the event-by-event 'head–tail' capability of the detector as a function of the energy of the recoil, the DMTPC collaboration introduced a quality factor $Q(E_R) = \epsilon(E_R) \times (1 - 2w(E_R))^2$, where ϵ is the recoil reconstruction efficiency and w is the fraction of wrong 'head–tail' assignments. The Q factor represents the effective fraction of reconstructed recoils with head–tail information, and the error on the head–tail asymmetry scales as $1/\sqrt{(Q)}$. Early measurements demonstrated a Q factor of 20% at 100 keV and 80% at 200 keV [51].

The DMTPC collaboration is currently designing a 1 m^3 detector. The apparatus consists of a stainless steel vessel of 1.3 m diameter and 1.2 m height. Nine CCD cameras and nine PMTs are mounted on each of the top and bottom plates of the vessel, separated from the active volume of the detector by an acrylic window. The detector consists of two optically separated regions. Each of these regions is equipped with a triple-mesh amplification device, located between two symmetric drift regions. Each drift region has a diameter of 1.2 m and a height of 25 cm, for a total active volume of 1 m^3. A field cage made of stainless steel rings keeps the uniformity of the electric field within 1% in the fiducial volume. A gas system recirculates and purifies the CF_4.

When operating the detector at a pressure of 50 Torr, a 1 m^3 module will contain 250 g of CF_4. Assuming a nuclear recoil energy threshold of 50 keV and an overall data-taking efficiency of 50%, a one-year underground run will yield an exposure of 45 kg-days. Assuming negligible backgrounds, such an exposure will allow the DMTPC experiment to set limits on spin-dependent interactions on protons of $\approx 10^{-39}$–10^{-38}, improving on current limits by about a factor of 50 [51].

5. Conclusion

Directional detectors can provide an unambiguous positive observation of DM particles even in presence of insidious backgrounds, such as neutrons or neutrinos. Moreover, the dynamics of the galactic DM halo will be revealed by measuring the direction of the incoming WIMPs, opening the path to WIMP astronomy.

In the past decade, several groups have investigated new ideas to develop directional DM detectors. Low-pressure TPCs are best suited for this purpose if an accurate (sub-millimeter) 3D reconstruction of the nuclear recoil can be achieved. A good tracking resolution also allows for an effective rejection of all electromagnetic backgrounds, in addition to statistical discrimination against neutrinos and neutrons based on the directional signature. The choice of different

gaseous targets makes these detectors well suited for the study of both spin-dependent (CS_2) or spin-independent (CF_4 and ^{3}He) interactions.

A vigorous R&D program has explored both electronic and optical readout solutions, demonstrating that both technologies can effectively and efficiently reconstruct the energy and vector direction of the nuclear recoils expected from DM interactions. The challenge for the field of directional DM detection is now to develop and deploy very sensitive and yet inexpensive readout solutions, which will make large directional detectors financially viable.

Acknowledgments

The authors are grateful to D Dujmic and M Morii for useful discussions and for proofreading the manuscript. GS is supported by the MIT Physics Department and the US Department of Energy (contract number DE-FG02-05ER41360). CJM is supported by Fermilab.

References

[1] Hinshaw G *et al* 2009 *Astrophys. J. Suppl.* **180** 225
[2] Lee B W and Weinberg S 1977 *Phys. Rev. Lett.* **39** 165–8
[3] Weinberg S 1982 *Phys. Rev. Lett.* **48** 1303–6
[4] Jungman G, Kamionkowski M and Griest K 1996 *Phys. Rep.* **267** 195
[5] Monroe J and Fisher P 2007 *Phys. Rev.* D **76** 033007
[6] Mei D and Hime A 2006 *Phys. Rev.* D **73** 053004
[7] Smith P F and Lewin J D 1990 *Phys. Rep.* **187** 203–80
[8] Drukier A K, Freese K and Spergel D N 1986 *Phys. Rev.* D **33** 3495
[9] Bernabei R *et al* (DAMA Collaboration) 2008 *Eur. Phys. J.* C **56** 333
[10] Spergel D N 1988 *Phys. Rev.* D **37** 1353
[11] Copi C J, Heo J and Krauss L M 1999 *Phys. Lett.* B **461** 43
[12] Vergados J D 2003 *Phys. Rev.* D **67** 103003
[13] Morgan B, Green A M and Spooner N J C 2005 *Phys. Rev.* D **71** 103507
[14] Freese K, Gondolo P and Newberg H J 2005 *Phys. Rev.* D **71** 43516
[15] Alenazi M S and Gondolo P 2008 *Phys. Rev.* D **77** 043532
[16] Sikivie P 1999 *Phys. Rev.* D **60** 063501
[17] Tkachev I I and Wang Y 1997 *Phys. Rev.* D **56** 1863
[18] Sikivie P, Tkachev I I and Wang Y 1995 *Phys. Rev. Lett.* **75** 2911
[19] Green A M and Morgan B 2007 *Astropart. Phys.* **27** 142–9
[20] Smith M C *et al* 2007 *Mon. Not. R. Astron. Soc.* **379** 755
[21] Lindhard J, Scharff M and Schiott H 1963 *Kgl. Danske Vadenskab. Selskab, Mat. Fys. Medd.* **33** 14
[22] Lindhard J, Scharff M and Schiott H 1963 *Kgl. Danske Vadenskab. Selskab, Mat. Fys. Medd.* **33** 10
[23] White J T *et al* 2007 *Nucl. Phys.* B **173** 144
[24] Martin C *et al* 2009 Abstract G10-7 *APS April Meeting 2009* submitted
[25] Aprile E *et al* 2006 *Phys. Rev. Lett.* **97** 081302
[26] Ziegler J F *SRIM—The Stopping and Range of Ions in Matter* www.srim.org
[27] Bohr N, Lindhard J and Dan K 1954 *Kgl. Danske Vadenskab. Selskab, Mat. Fys. Medd.* **28** 7
[28] Hitachi A 2008 *Radiat. Phys. Chem.* **77** 1311–7
[29] Ziegler J F, Biersack J P and Littmark U 1985 *The Stopping and Range of Ions in Solids* 1st edn (New York: Pergamon)
[30] Sigmund P 2004 *Stopping of Heavy Ions—A Theoretical Approach* (Springer Tracts in Modern Physics, vol 204)

[31] Paul H and Schinner A 2003 *At. Data Nucl. Data Tables* **85** 377
[32] Evans G E, Stier P M and Barnett C F 1953 *Phys. Rev.* **90** 825
[33] Lassen N O *et al* 1964 *Kgl. Danske Vadenskab. Selskab, Mat. Fys. Medd.* **34** 5
[34] Cano G L 1968 *Phys. Rev.* **169** 278
[35] Snowden-Ifft D P *et al* 2003 *Nucl. Instrum. Methods* A **498** 155–64
[36] Lewin J D and Smith P F 1996 *Astropart. Phys.* **6** 87–112
[37] Cano G L and Dressel R W 1965 *Phys. Rev.* A **139** 1883
[38] Stone W G and Cochrane L W 1957 *Phys. Rev.* **107** 702
[39] Phipps J A, Boring J W and Lowry R A 1964 *Phys. Rev.* A **135** 36
[40] Boring J W, Strohl G E and Woods F R 1965 *Phys. Rev.* A **140** 1065
[41] Mc Donald J R and Sideneus G 1969 *Phys. Lett.* A **28** 543
[42] Price J L *et al* 1993 *Phys. Rev.* A **47** 2913
[43] Bandler S R *et al* 1995 *Phys. Rev. Lett.* **74** 3169
[44] Martoff C J *et al* 1996 *Phys. Rev. Lett.* **76** 4882
[45] Natsume M *et al* 2007 *Nucl. Instrum. Methods* A **575** 439–43
[46] Nygren D R 1975 *PEP-0144, Proc. PEP Summer Study* (Berkeley, CA) p 58
[47] Fancher D *et al* 1979 *Nucl. Instrum. Methods* **161** 383
[48] Snowden-Ifft D P, Martoff C J and Burwell J M 2000 *Phys. Rev.* D **61** 101301
[49] Sciolla G *et al* (DMTPC Collaboration) 2009 arXiv:0903.3895 (astro-ph)
[50] Miuchi K *et al* (NEWAGE Collaboration) 2007 *Phys. Lett.* B **654** 58
[51] Dujmic D *et al* (DMTPC Collaboration) 2008 *Astropart. Phys.* **30** 58
[52] Rolandi L and Blum W 1994 *Particle Detection with Drift Chambers* (Berlin: Springer)
[53] Sauli F 1987 *Experimental Techniques in High Energy Physics* ed T Ferbel (Reading, MA: Addison-Wesley) p 81
[54] Caldwell T *et al* (DMTPC Collaboration) 2009 arXiv:0905.2549 (physics.ins-det)
[55] Martoff C J *et al* 2000 *Nucl. Instrum. Methods* A **440** 355–9
[56] Martoff C J *et al* 2009 *Nucl. Instrum. Methods* A **598** 501–4
[57] Ohnuki T, Martoff C J and Snowden-Ifft D P 2001 *Nucl. Instrum. Methods* A **463** 142–8
[58] Dion M P 2009 *PhD Dissertation* Temple University Physics (available online through ProQuest Dissertations and Theses database)
Dion M P, Martoff C J and Hosack M 2009 On the mechanism of Townsend avalanche for negative molecular ions (arXiv:0908.2441)
[59] Angle J *et al* (XENON Collaboration) 2008 *Phys. Rev. Lett.* **100** 1303
[60] Ahmed Z *et al* (CDMS Collaboration) 2009 *Phys. Rev. Lett.* **102** 1301
[61] Arisaka K *et al* 2009 *Astropart. Phys.* **31** 63
[62] Gerbier G 1990 *Nucl. Phys.* B **13** 207–8
[63] Buckland K N *et al* 1994 *Phys. Rev. Lett.* **73** 1067–70
[64] Lehner M J, Buckland K N and Masek G E 1997 *Astropart. Phys.* **8** 43–50
[65] Alner G J *et al* (DRIFT Collaboration) 2004 *Nucl. Instrum. Methods* A **535** 644
[66] Lawson T B *et al* (DRIFT-II Collaboration) 2005 *Nucl. Instrum. Methods* A **555** 173–83
[67] Burgos S *et al* (DRIFT-II Collaboration) 2007 *Astropart. Phys.* **28** 409
[68] Burgos S *et al* (DRIFT-II Collaboration) 2009 *Nucl. Instrum. Methods* A **600** 417
[69] Boston A J *et al* 2005 *Nucl. Instrum. Methods* A **573** 1–322
[70] Black J K *et al* 2007 *Nucl. Instrum. Methods* A **581** 755
[71] Amendolia S R *et al* 1999 *Nucl. Instrum. Methods* A **422** 201
[72] Sauli F 1997 *Nucl. Instrum. Methods* A **386** 531
[73] Giomataris Y *et al* 1996 *Nucl. Instrum. Methods* A **376** 29
[74] Amsler C *et al* 1997 *Nucl. Instrum. Methods* A **396** 115
[75] Dujmic D *et al* (DMTPC Collaboration) 2008 *Nucl. Instrum. Methods* A **584** 327

[76] Christophorou L G *et al* 1996 *J. Phys. Chem. Ref. Data* **25** 1341
[77] Ellis R J and Flores R A 1991 *Phys. Lett.* B **263** 259
[78] Pansky A *et al* 1995 *Nucl. Instrum. Methods* A **354** 262–9
[79] Kaboth A *et al* (DMTPC Collaboration) 2008 *Nucl. Instrum. Methods* A **592** 63–72
[80] Fraga M M F R *et al* 2003 *Nucl. Instrum. Methods* A **504** 88–92
[81] Kubo H *et al* (NEWAGE Collaboration) 2003 *Nucl. Instrum. Methods* A **513** 94
[82] Tanimori T *et al* 2004 *Phys. Lett.* B **578** 241
[83] Miuchi K *et al* (NEWAGE Collaboration) 2007 *Nucl. Instrum. Methods* A **576** 43
[84] Santos D *et al J. Phys.: Conf. Ser.* **65** 012012
[85] Guillaudin O *et al* 2009 arXiv:0904.1667
[86] Sciolla G *et al* (DMTPC Collaboration) 2008 arXiv:0811.2922
[87] Sciolla G 2008 arXiv:0811.2764
[88] Dujmic D *et al* (DMTPC Collaboration) 2008 arXiv:0810.2769
[89] Dujmic D *et al* (DMTPC Collaboration) 2008 *J. Phys.: Conf. Ser.* **120** 042030